Advanced Steel Construction – Vol. 21 No. 3 (2025) 194–203
DOI:10.18057/IJASC.2025.21.3.2

STUDY ON SHEAR BEHAVIOR OF T-SHAPED SHEAR CONNECTORS IN PREFABRICATED CONCRETE COMPOSITE FLOOR SLAB

Zeng-Mei Qiu *, Wen-Zhuang Pei, Guo-Chang Li and Zhi-Jian Yang

School of Civil Engineering, Shenyang Jianzhu University, Shenyang 110168, China

* *(Corresponding author: E-mail: qzmfighting@126.com)*

A B S T R A C T

This study proposed to apply T-shaped shear connectors to join prefabricated concrete slabs with H-beams and thereby ensure the overall working performance of building floor systems. The push-out tests on T-shaped connector specimens with different flange and web thicknesses were conducted aiming to investigate the shear behavior of this connector. Then the finite element software ABAQUS was used to establish test models, and the accuracy of the established models were verified according to the comparative experimental results to analyze the stress development process and key parameters influencing connector shear behavior. The results showed that the T-shaped connector with high initial stiffness and shear capacity, and its characteristic displacement complied with the lower limit value of permissible slip specified for the flexible shear connector in Eurocode 4, confirming its excellent ductility. The connector web thickness had the greatest effect on shear capacity, the second was the steel yield strength, whereas the connector width had the least influence. Finally, the recommended cross-sectional dimensions for the T-shaped connector were given, as well as the shear bearing capacity equation for this connector was derived, which could provide theoretical basis and design suggestions for its application in prefabricated concrete composite floor structure.

A R T I C L E   H I S T O R Y

Received: 28 November 2024
Revised: 27 December 2024
Accepted: 1 January 2025

K E Y W O R D S

Prefabricated concrete composite floor slabs;
Push-out test;
T-shaped shear connector;
Shear behavior;
Finite element simulation

1. Introduction

The prefabricated steel structure–composite slab system offers advantages such as rapid constructability, controllable quality, and structural stability [1]. The prefabricated concrete floor slab of this system has been widely applied as it provides excellent integrity, suitable crack resistance, and high stiffness while realizing a large net interior space. As a result, prefabricated slabs have become one of the widely used floor forms in composite steel structures [2]. However, the bond between the prefabricated floor slab and steel beam is insufficient to bear the longitudinal shear force generated under large load. Therefore, shear connectors must be set between them to ensure the integrated working performance of composite system [3].

The primary function of a shear connector is to resist the longitudinal shear and horizontal uplifting force between the prefabricated floor slab and supporting section steel [4]. Studs are the traditional form of shear connector and are widely used in practical engineering applications [5-6]. However, with the rapid development of composite structures, scholars from all over the world have successively proposed different forms of shear connectors and applied them to various building structures, including perforated Perfobond Leisten (PBL) shear connector as well as truss shear connector, channel steel, and angle steel. Notably, the angle steel connector can be provided in more configurations, realizes more convenient construction, uses less material, exhibits superior shear behavior compared to the channel steel connector, and the mechanical performances of its connection can be guaranteed by fixing the steel plate on to the flange of steel beam using a fillet weld applied by conventional welding equipment; as a result, the angle steel connector is widely applied in structures with high shear capacity requirements [7].

At present, numerous researchers have studied various aspects of angle shear connectors. For example, Viest et al. [8] firstly performed the push-out and bending tests of channel steel connectors in the 1950s, providing a valuable reference for the subsequent research of assorted section steel connectors. Based on the results of monotonic push-out and cyclic loading tests, Shariat et al. [9] observed that the shear capacity of angle steel were lower than that of channel steel, but the shorter angle connectors and longer channel connectors exhibited superior ductility. Furthermore, Haroon et al. [10]、Arévalo et al. [11] and Hajime et al. [12] respectively analyzed the section size, arrangement angle steel connectors and arrangement spacing of angle connectors, and put forward some corresponding design suggestions. Zhou et al. [13] conducted push-out tests of angle steel and determined that the equation provided by American Code for calculating the bearing capacity was too conservative; they proposed an empirical equation for shear bearing capacity that is suitable for concrete strengths greater than 20 MPa and connector thicknesses greater than 6 mm. Notably, Cui et al. [14] conducted beam tests indicating that angle steel connectors can replace slab reinforcement; concrete slabs welded with angle connectors exhibited excellent overall performance with higher stiffness and lower cost than traditional prefabricated slabs. Tang et al. [15] experimentally and theoretically determined that the connection position of the upper flange of steel beam and angle steel connector in a tunnel structure was prone to concrete void formation, and this phenomenon will seriously affect the shear stiffness and bearing capacity of the angle steel, but improved its deformation capacity. In addition, a few scholars have studied other forms of connection. Soty et al. [16] found that the thickness to height ratio of shear connectors and orientation angle of L-shaped connectors would affect the final failure form and shear resistance mechanism of L-shaped connectors, considered the effect on material strength, connector size, and orientation angle on its shear capacity. Wang et al. [17] analyzed the mechanical performances of angle steel, channel steel and T-shaped PBL connectors under repeated loading, and found that the stiffness of them decreased continuously; the PBL connector exhibited particularly obvious shear stiffness degradation.

Unlike prior studies on angle or channel steel connectors, this study focuses on T-shaped shear connectors, which offer advantages in ductility, stiffness, and ease of construction, as well as provide a long welding length and large contact area with the H-beam that result in strong shear and uplift resistance (see Fig. 1). Various T-shaped shear connector configurations with different web and flange thicknesses were accordingly subjected to push-out tests to determine their failure modes, whole loading process and load–slip curves. These results were subsequently applied to verify finite element simulation and further analyze the influence of the component sizes of T-shaped connector and material strength on the shear behaviors of the connectors. Finally, the shear bearing capacity calculation formula of the T-shaped connector was put for word according to the simulation results, providing a reference for the application of this connector in future buildings.

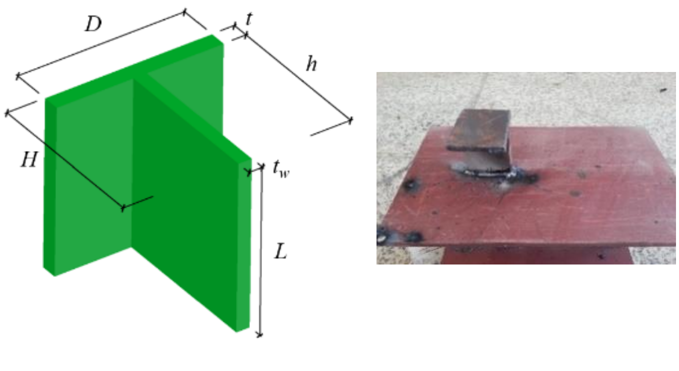

Fig. 1 T-shaped shear connector

2. Experiment materials and methods

2.1. Specimen design

According to EN 1994-1-1(EC 4) [18], the design of test specimens was shown in Fig. 2. Each specimen comprised a 300 mm × 300 mm × 10 mm × 15 mm H-beam, 500 mm × 150 mm × 400 mm concrete slab (cast-in-place and prefabricated), and 700 mm × 350 mm × 100 mm cast-in-place concrete base. An end plate is welded at the loading position of H-beam to make that the components are stressed uniformly in the loading project, and the size is 350 mm × 35 0mm × 20 mm. In this test, the thickness of the shear connector flange and web plate were the influencing factors, resulting in eight specimens in the four groups detailed in Table 1.

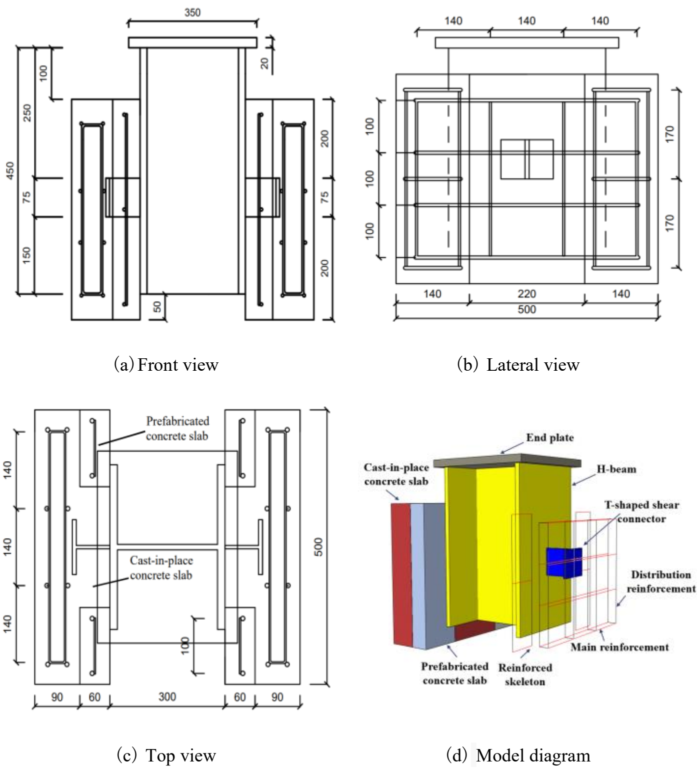

(a) Front view (b) Lateral view

(c) Top view (d) Model diagram

Fig. 2 Test specimen dimensions and structural diagram

Table 1
Parameters of tested T-shaped shear connectors

Specimen number	H (mm)	D (mm)	L (mm)	t_w (mm)	t (mm)	l_w (mm)
TG-1	100	100	75	6	8	75
TG-2	100	100	75	6	8	75
TG-3	100	100	75	8	8	75
TG-4	100	100	75	8	8	75
TG-5	100	100	75	6	10	75
TG-6	100	100	75	6	10	75
TG-7	100	100	75	8	10	75
TG-8	100	100	75	8	10	75

Note: H, D and L are the height, width and length of the T-shaped connector, respectively; t_w is the web thickness; t is the flange thickness; l_w is the weld length.

2.2. Material properties

Table 2 lists the material parameters of the steel components: the T-shaped shear connectors, H-beams, and end plates were all made of Q235B grade steel. The slab reinforcement was made of HPB300 grade steel with ϕ8 threaded bars in the stressed direction and ϕ6 threaded bars in the distributed direction. The prefabricated slab was made of C30 concrete, and the cast-in-place slab and base were made of C45 concrete; According to compressive strength test of concrete cube (150mm). The average compressive strength of C30 concrete was 30.0 MPa and its elastic modulus was $3.00×10^4$ MPa; the average compressive strength of C45 concrete was 45.3 MPa and its elastic modulus was $3.35×10^4$ MPa.

Table 2
Material properties of steel

Thickness of steel plate(mm)	Type	f_y(MPa)	f_u(MPa)	E_s(GPa)
6	Q235B	413.3	480.0	206
8	Q235B	425.6	483.7	204

Note: f_y, f_u and E_s are the yield strength, tensile strength and elastic modulus of steel, respectively.

2.3. Loading device and scheme

A 100t jack was selected for force loading in the test as shown in Fig. 3. The loading scheme comprised a monotonic concentrated-load static test with preloading and formal loading stages. This scheme was consistent with that used in [19].

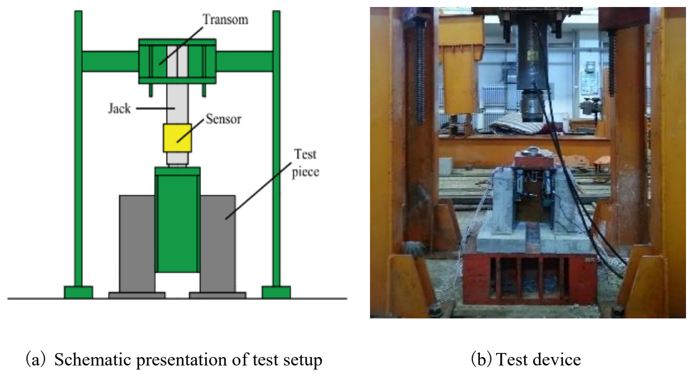

(a) Schematic presentation of test setup (b) Test device

Fig. 3 Test setup

2.4. Measurement system

The response of each specimen to the applied load was determined by measuring its strain and deformation. Fig. 4 (a) depicts the arrangement of the connector strain gauges. Strain rosette T1 was located on the web of T-shaped connector, near the weld at the flange of H-beam, rosette T2 was located in the middle of the web, and rosettes T3–T5 were located on both sides and at the middle of the flange. The equivalent strain values for the rosettes were calculated from the strain values in three directions [19]. Fig. 4 (b) depicts the displacement meter arrangement. In order to obtain the relative slip value between H-beam and T-shaped connector as well as the vertical displacement of H-beam relative to composite slab, two displacement meters were placed in the middle of the H-beam, one parallel and one perpendicular to the weld between the connector and H-beam.

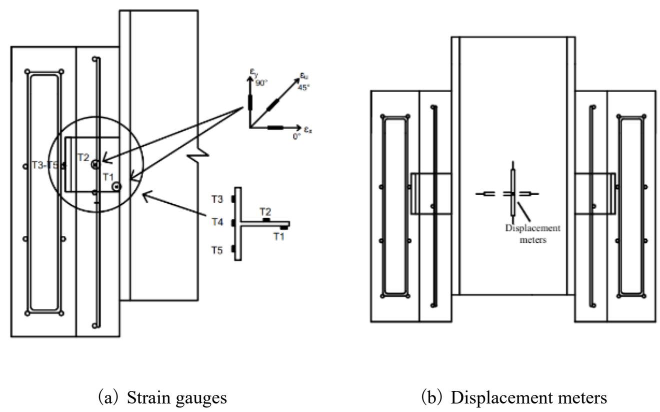

(a) Strain gauges (b) Displacement meters

Fig. 4 Measurement layout

3. Experiment results

3.1. Test phenomena and failure modes

The failure modes of the specimens with different parameters were similar, exhibiting an obvious slip between the prefabricated concrete floor slab and H-beam. Failure occurred at the weld between the H-beam and T-shaped shear connector, accompanied by wide cracks in the nearby concrete slab.

The observed test phenomena are described in this section considering TG-8 as a typical specimen. The specimen showed no obvious change in the initial loading stage. The first crack appeared on the CR-1 plane when the load reached 75% of the peak value (see Fig. 5(a)). The length and width of this crack gradually extended with further increase in load, followed by the appearance of a second crack on the C-1 plane (see Fig. 5(b)). The specimen suddenly exhibited a large displacement when the peak load was achieved, at which time a third crack appeared on the C-2 plane and multiple microcracks appeared near the second and third cracks (see Fig. 5(c)). As the contact surface between the concrete slab and H-beam was completely disconnected at this time, the loading was stopped. The observed crack pattern of the specimen presented local spalling of the concrete slab on plane C-2 (see Fig. 5(d)). The maximum crack widths of 1.5 and 0.9 mm on planes CR-1 and C-1, respectively, a number of 0.12–0.35 mm wide microcracks between the concrete slab and T-shaped connector on the C-2 surface, and a fourth crack on the concrete base that was only 0.15 mm wide.

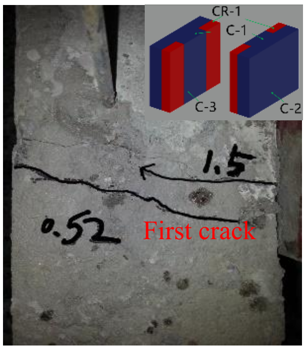

(a) CR-1 plane fracture

(b)C-1 plane fracture

(c) C-2 plane fracture

(d) The concrete block on side C-2 falls off

Fig. 5 Specimen failure mode

3.2. Load-slip curves

Fig. 6 shows the comparison of load-slip (P–δ) curves of specimens. Each group of specimens reached yield at 70–75% of their peak load. Different degrees of fracture appeared between the prefabricated floor slab and H-beam at peak load, the loading was stopped, and the slip value increased slowly with the subsequent decrease in applied load. The characteristic slip values for the specimens were within 15.67–30.56 mm, exceeding the lower limit for flexible connectors in Eurocode 4 (> 6 mm) [18]. When the connector web thickness was 6 mm, a thicker flange increased the yield and peak loads; the yield and peak loads of TG-5 were 11.6% and 24.4% higher, respectively, than those of TG-2. When the web thickness was 8 mm, the change of flange thickness had little effect on its yield load, but its peak load increased by 15.4%. When the flange thickness was 8 mm, the yield and peak loads increased by 30.6% and 21.4% with the increase of web thickness, respectively, and when it was 10 mm, by 22.7% and 13.5%.

The ultimate shear capacity versus ductility coefficient (D_c) curves shown in Fig. 7 [20]. The D_c values of each specimen were 39.2, 21.8, 94.5, and 61.3. After reaching the yield load, each P–δ curve exhibits a long plateau, indicating excellent ductility. Changing the flange thickness had a great effect on the D_c: when the web thickness was 6 mm and 8 mm, an increase in flange thickness from 8 mm to 10 mm increased the D_c value by 2.4 times and 2.8 times, respectively. Compared with traditional bolted connectors [21], its D_c values were within 1.97-2.07, while the D_c values of T-shaped shear connectors were within 21.8-94.5, indicating that T-shaped shear connectors have better ductility.

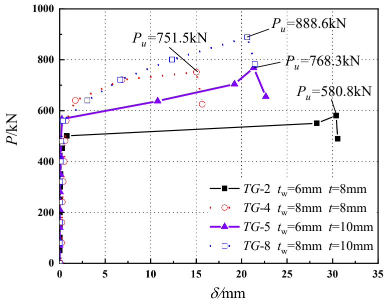

Fig. 6 Load–slip curves

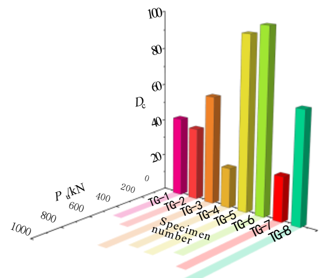

Fig. 7 Ultimate shear capacity–ductility coefficient curves

3.3. Load-strain curves

Fig. 8 compares the load-strain curves of the evaluated specimens, and the strain value was negative under compression and positive under tension. The curves for rosettes T1 and T2 exhibit the same trends in each group, and the strain in the connector flange of each group exhibited no obvious change during the entire loading process, indicating that no yield phenomenon occurred within. The connector webs were consistently in tension, and the bottom of the web connecting with the H-beam was the first to yield. The yield strain was attained at the center of the connector webs in specimens TG-2 and TG-5, but not at those in specimens TG-4 and TG-8. This phenomenon indicates that an increase in web thickness can effectively delay the yield of the shear connector, whereas an increase in flange thickness has little influence.

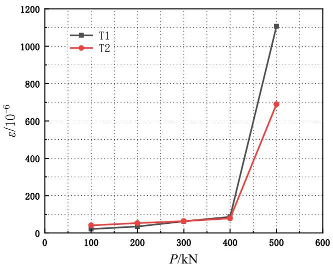

(a)TG-2

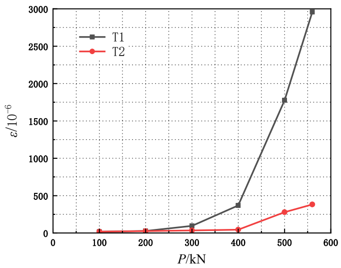

(b)TG-4

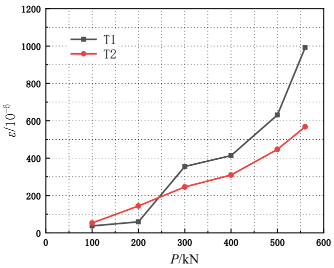

(c)TG-5

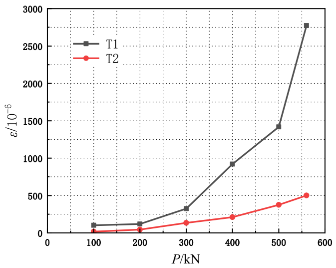

(d)TG-8

Fig. 8 Load–strain curves

4. Finite element analysis

4.1. Model establishment and verification

The finite element analysis (FEA) software ABAQUS was used to perform refined and expanded numerical simulations evaluating the shear behavior of T-shaped connector specimens subjected to push-out loading.

4.1.1. Material constitutive models

For concrete, the concrete plastic damage model provided in ABAQUS was selected for analysis. As shown in Fig. 9 (a), the inelastic stage was defined using the stress–strain curve provided in the Code for design of concrete structures [22]. The double-fold elastic–plastic constitutive model was defined for the steel material [23] as shown in Fig. 9 (b).

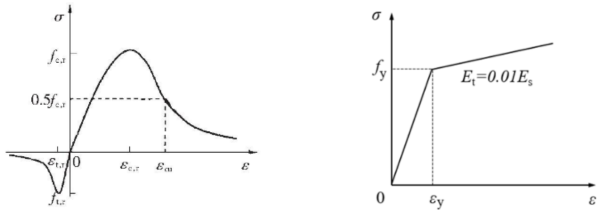

(a) Stress-strain curve of concrete (b) Stress-strain curve of steel

Fig. 9 Material constitutive models

4.1.2. Finite element type and component mesh division

The FEA model established in this study comprised a prefabricated concrete slab, cast-in-place concrete slab, H-beam, T-shaped shear connector, and steel reinforcement; the geometric size of each component was consistent with those of the push-out specimen evaluated in Section 3. The concrete slabs, H-beam, and T-shaped shear connector components were modeled using the C3D8R reduced integral eight-node solid element; the reinforcement bars were modeled using the T3D2 truss element [24]. The general mesh division in the model was 20 mm with a refined mesh of 10 mm at locations where the stress was concentrated, such as the T-shaped connector and the opening of cast-in-place concrete slab, to accurately simulate the stress development process while limiting the computational burden and facilitating model convergence. The complete mesh is shown in Fig. 10.

4.1.3. Boundary conditions and loading methods

Binding constraint was applied between the prefabricated concrete slab and cast-in-place concrete slab and between the H-beam and T-shaped shear connector. Hard contact was applied between the prefabricated floor slab and H-beam. Surface-to-surface contact was applied between the cast-in-place concrete slab and H-beam and between the cast-in-place concrete slab and T-shaped shear connector with penalty friction [25-26] coefficients of 0.2 and 0.4, respectively, in the tangential direction. Embedded constrain was applied to the reinforcement. The bottoms of the cast-in-place and prefabricated concrete slab were completely fixed, and the upper surface of H-beam was coupled to simulate the applied displacement loading. The completed FEA model is shown in Fig. 10.

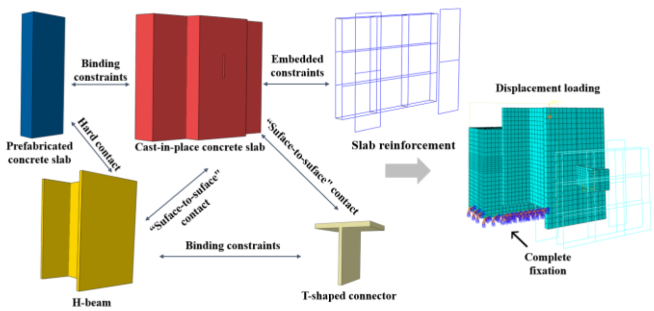

Fig. 10 FEA model boundary conditions and mesh division

4.1.4. Model validation

The test and FEA-obtained P–δ curves are compared in Fig. 11 and the detailed results are provided in Table 3. The P–δ curves obtained by the FEA simulation were basically consistent with those determined by testing, showing relative errors of less than 10% between peak loads, confirming the accuracy of the FEA modeling approach.

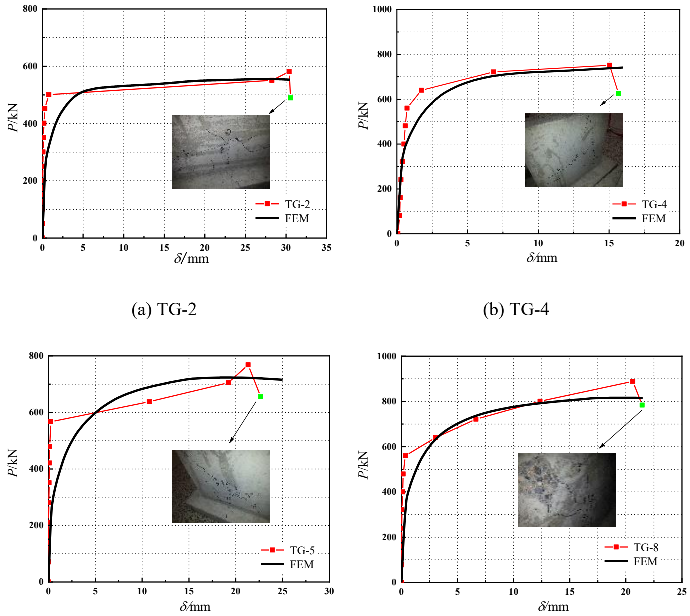

(a) TG-2 (b) TG-4

(c) TG-5 (d) TG-8

Fig. 11 Comparison of test and FEA-obtained P–δ curves

Table 3
Comparison of test and FEA-obtained results

Specimen number	Test Results		Simulation results	$P_{u,s}/P_{u,t}$
	$P_{u,t}$(kN)	Mean value	$P_{u,s}$(kN)	
TG-1	511.4	546.1	555.61	1.02
TG-2	580.8			
TG-3	848.1	799.8	747	0.93
TG-4	751.5			
TG-5	768.3	725.4	726.99	1.0
TG-6	682.5			
TG-7	797.8	843.2	820.36	0.97
TG-8	888.6			

Note: $P_{u,t}$ and $P_{u,s}$ are the shear bearing capacity obtained by test and numerical simulation, respectively.

4.2. Analysis of the stress development process

The numerical analysis model of specimen TG-2 is used as an example in this discussion of the stress development process. As shown in Fig. 12, the FEA-obtained P–δ curve can be divided into three stages between points O, A, B, and C: the elastic working stage in segment OA, elastic–plastic working stage in segment AB, and strengthening stage in segment BC. Point O denotes the beginning of loading, point A denotes when the T-shaped connector reaches the yield load, point B denotes as the entire section at the bottom of the web reaches the tensile limit (i.e., strain rosettes T1 and T2 fail), and point C denotes when the shear connector reaches its peak load ($P_{u,t}$) and loading is stopped. The stress and strain nephograms of each component at these characteristic points are shown in Figs. 13–15.

In segment OA, the connector is within the elastic working range, and the initial stiffness of the specimen was large. When the curve reached point A, considerable stress was present at the weld between the H-beam and connector (see Fig. 13(b)) and extrusion contact occurred between the side of the web of connector close to H-beam and the cast-in-place concrete slab, which slab experienced large local strain, while the prefabricated concrete slab experienced almost no strain (see Fig. 13(c)). The shear connector began to yield locally from the lower part at the position of the welding surface between the web and H-beam (see Fig. 13(d)) when the load was 0.49 $P_{u,t}$ and the displacement was 0.42 mm.

Next, the specimen entered the elastic–plastic working stage in segment AB. At point B, the stress at the weld between the bottom of the shear connector and H-beam was close to the yield value (see Fig. 14(b)), corresponding to the considerable compressive strain in the concrete slab at the shear connector web, which locally exceeded the ultimate compressive strain by 0.0033, indicating concrete slab cracking (see Fig. 14(c)). Furthermore, the entire bottom section of the connector web reached the ultimate tensile stress (480 MPa). At this time, obvious shear deformation appeared at the weld joint, and the shear force was transmitted to the flange plate from the web plate, and the stress began to occur at the connection position between the flange and the web (Figure 14d).

Finally, the specimen entered the strengthening stage in segment BC. At point C, the stress in the middle-lower part of the weld between T-shaped connector and H-beam reached yield (Fig. 15(b)), and the concrete slab below the connector web reached the ultimate compressive strain. At this time, the concrete slab was crushed, which coincided with the observed experimental phenomenon (Fig. 15(c)), the top of the joint between T-shaped connector flange and web yielded locally, also the web completely reached the ultimate tensile stress from the side near the H-beam to the middle. Eventually the connection lost its shear capacity (see Fig. 15(d)).

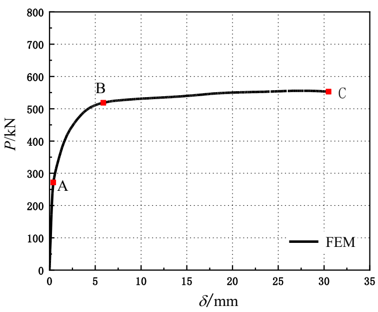

Fig. 12 TG-2 load–slip curve

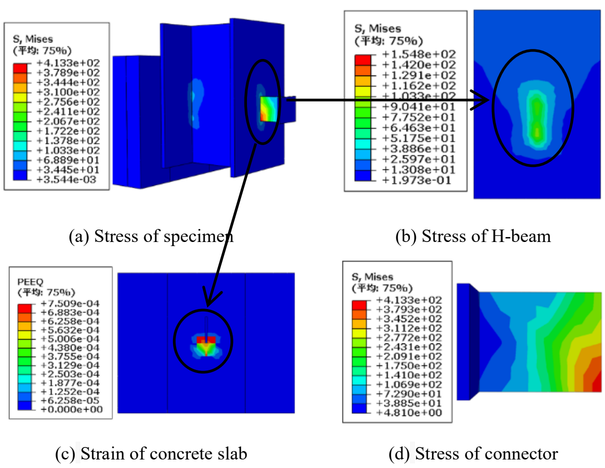

(a) Stress of specimen (b) Stress of H-beam

(c) Strain of concrete slab (d) Stress of connector

Fig. 13 Stress and strain in each part of TG-2 at point A

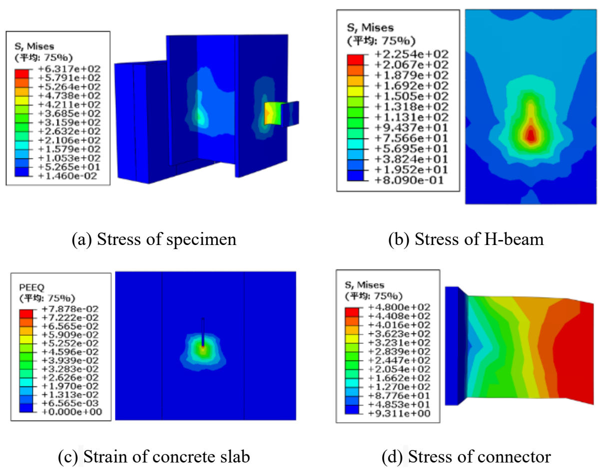

(a) Stress of specimen (b) Stress of H-beam

(c) Strain of concrete slab (d) Stress of connector

Fig. 14 Stress and strain in each part of TG-2 at point B

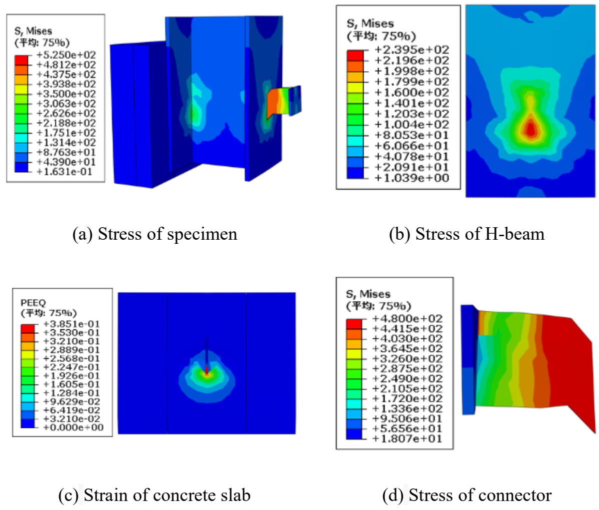

(a) Stress of specimen (b) Stress of H-beam

(c) Strain of concrete slab (d) Stress of connector

Fig. 15 Stress and strain in each part of TG-2 at point C

4.3. Extended parameter analysis

The influence law of different parameters on shear behavior of the T-shaped shear connector was further investigated using 48 numerical models with web thicknesses t_w of 6–14 mm, flange thicknesses t of 6–14 mm, connector lengths L of 65–95 mm, web heights h of 42–92 mm, connector widths D of 80–110 mm, prefabricated concrete compressive strength f_{cu}' of 30–70 MPa, cast-in-place concrete compressive strength f_{cu} of 30–70 MPa, and steel yield strengths f_y of 235–460 MPa, as detailed in Table 4.

4.3.1. Effect of web thickness

The bearing capacity of T-shaped connector increased slightly as t_w was increased from 6 to 7 mm, then increased in an approximately linear fashion at an average rate of 6.5% when t_w was increased from 7 to 13 mm, and finally decreased when t_w was increased from 13 to 14 mm (see Fig. 16(a)). Therefore, increasing the web thickness within a specified scope can effectively enhance the shear capacity of this connector, but it should not exceed 13 mm.

4.3.2. Effect of flange thickness

The bearing capacity of T-shaped connector continuously improved as t was increased from 6 to 11 mm, then decreased at higher thicknesses (see Fig. 16(b)). The primary reason for this change was that the increase in load began to transmit the shear force through the web to flange. Once the web completely yielded from the bottom near the H-beam, the load could not be effectively transmitted to the flange, causing the impact of changing t on the bearing capacity of the connector to gradually reduce. These results suggest that the flange thickness should not exceed 11 mm.

4.3.3. Effect of connector length

The bearing capacity of T-shaped connector improved as L was increased from 65 to 95 mm, and its most significant improvement of 10.2% occurred with the increase in L from 85 to 95 mm (see Fig. 16(c)). The primary reason for this result was that a longer connector increased the weld area, effectively improving the shear capacity of the connection.

4.3.4. Effect of web height

The bearing capacity of T-shaped connector increased by 9.9% and 14.1% when h was increased from 42 to 52 mm and 62 mm, respectively, above which further increase in h had no significant effect (see Fig. 16(d)). Therefore, it indicates that increasing the web height in a certain range has almost no impact on the bearing capacity, and it is recommended that the web height need not exceed 62 mm.

4.3.5. Effect of connector width

The bearing capacity of T-shaped connector only increased by 0.2% when D was increased from 80 to 90 mm, and improved only slightly more when it was increased to 100 mm (see Fig. 16(e)). Therefore, the connector width has little influence on its shear capacity, and can be set as required to satisfy the structural design requirements, particularly regarding the required lifting resistance.

4.3.6. Effect of prefabricated concrete compressive strength

When f_{cu}' was between 30 MPa and 70 MPa, its shear capacity enhanced negligibly, and only when f_{cu}' was increased from 30 to 40 MPa, its shear capacity enhanced by 2.1% (see Fig. 16(f)). Therefore, considering the effects on bearing capacity as well as economy, the strength of the prefabricated concrete should be 40 MPa.

4.3.7. Effect of cast-in-place concrete compressive strength

Increasing f_{cu} effectively improved the bearing capacity of T-shaped connector. The improvement effect of bearing capacity gradually decreased with increasing f_{cu} from 30 to 60 MPa, but remained generally consistent thereafter (see Fig. 16(g)). Therefore, the strength of the cast-in-place concrete need not exceed 60 MPa.

4.3.8. Effect of steel yield strength

The shear capacity of T-shaped connector increased by varying degrees with increasing f_y. Each subsequent increase in f_y from 235 to 275, 355, 390, 420, and 460 MPa increased the shear capacity by 4.9%, 6.4%, 2.4%, 2.6%, and 2.2%, respectively. (see Fig. 16(h)). Therefore, the optimal shear capacity can be realized using a connector steel strength of 355 MPa.

4.4. Design recommendations for T-shaped shear connectors

The results of parameter analysis obtained in Section 4.3 demonstrate that the web thickness, flange thickness, connector length, web height and material strength, all significantly influence the shear behavior of T-shaped connector. These results suggest that T-shaped connector designs should consider a web thickness less than 13 mm, flange thickness less than 11 mm, and web height less than 62 mm and should provide a connector width and length meeting the structural requirements of the Specifications for hot rolled section steel [27] and the Code for design of concrete structures [22]. Considering both economic and structural design requirements, the proposed size selection of a T-shaped shear connector is shown in Table 5.

Table 5
Size selection of T-shaped shear connector

Influencing parameter	Selection range	Optimum value
t_w(mm)	$6 \leqslant t_w \leqslant 13$	13
t(mm)	$6 \leqslant t \leqslant 11$	10
L(mm)	design requirements	75
h(mm)	$42 \leqslant h \leqslant 62$	62
D(mm)	design requirements	80

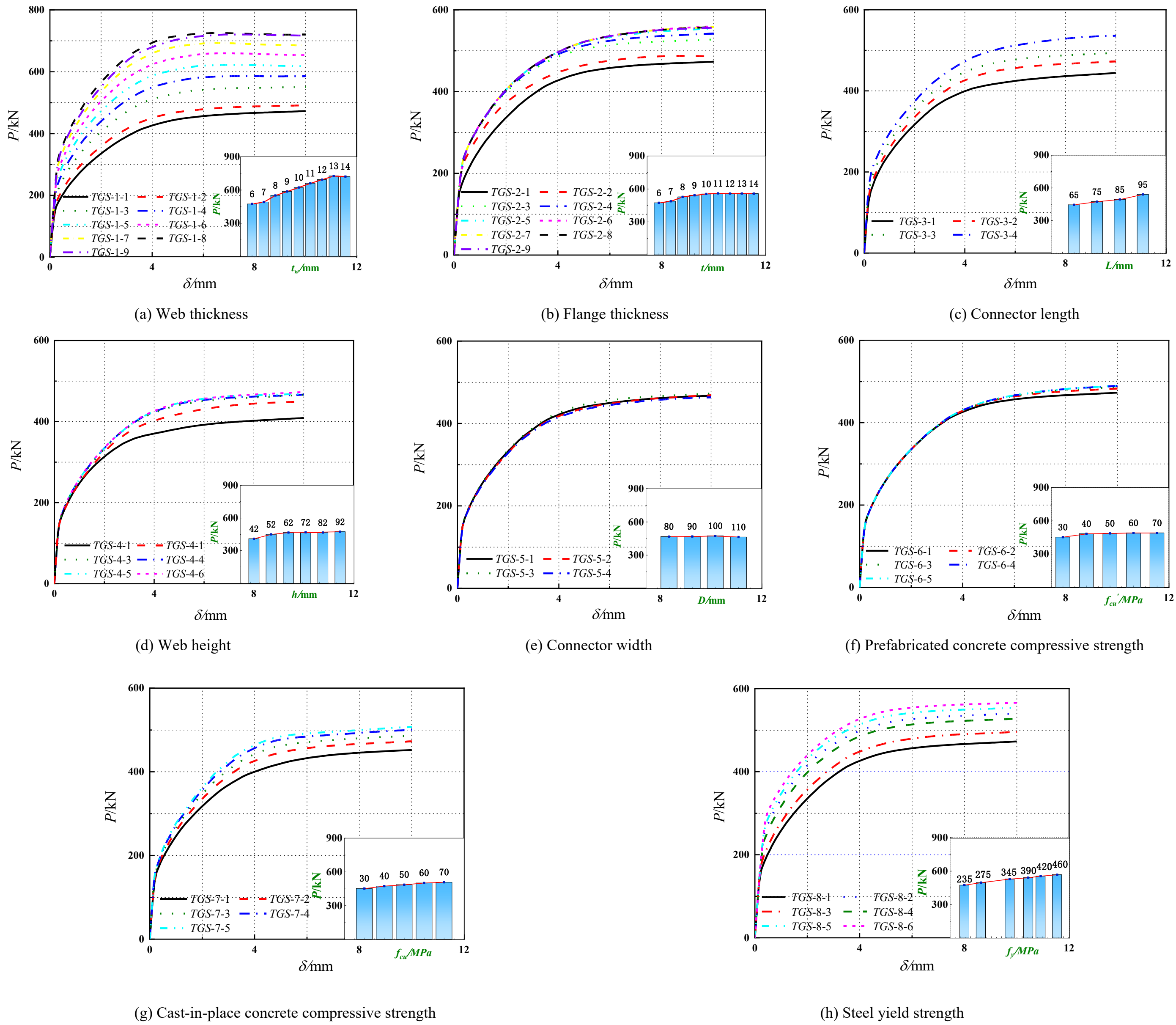

Fig. 16 Load-slip curves with different parameters

Table 4
Specimen details for FEA evaluation

Numerical model number	$H \times D \times L$(mm)	t_w(mm)	t(mm)	f_{cu}'(MPa)	f_{cu}(MPa)	f_y(MPa)	h(mm)	$P_{u,s}$(kN)
TGS-1-1	100×100×75	6	8	30	40	235	92	472.8
TGS-1-2	100×100×75	7	8	30	40	235	92	491.4
TGS-1-3	100×100×75	8	8	30	40	235	92	550.9
TGS-1-4	100×100×75	9	8	30	40	235	92	585.6
TGS-1-5	100×100×75	10	8	30	40	235	92	622.2
TGS-1-6	100×100×75	11	8	30	40	235	92	659.6
TGS-1-7	100×100×75	12	8	30	40	235	92	693.1
TGS-1-8	100×100×75	13	8	30	40	235	92	725.5
TGS-1-9	100×100×75	14	8	30	40	235	92	720.5
TGS-2-1	98×100×75	6	6	30	40	355	92	473.2
TGS-2-2	99×100×75	6	7	30	40	355	92	487.2
TGS-2-3	100×100×75	6	8	30	40	355	92	527.4
TGS-2-4	101×100×75	6	9	30	40	355	92	542.1
TGS-2-5	102×100×75	6	10	30	40	355	92	554.5
TGS-2-6	103×100×75	6	11	30	40	355	92	559.4
TGS-2-7	104×100×75	6	12	30	40	355	92	558.1
TGS-2-8	105×100×75	6	13	30	40	355	92	557.5
TGS-2-9	106×100×75	6	14	30	40	355	92	556.6
TGS-3-1	100×100×65	6	8	30	40	235	92	444.4
TGS-3-3	100×100×85	6	8	30	40	235	92	493.8
TGS-3-4	100×100×95	6	8	30	40	235	92	539.1
TGS-4-1	50×100×75	6	8	30	40	235	42	408.8
TGS-4-2	60×100×75	6	8	30	40	235	52	449.4
TGS-4-3	70×100×75	6	8	30	40	235	62	466.3
TGS-4-4	80×100×75	6	8	30	40	235	72	466.4
TGS-4-5	90×100×75	6	8	30	40	235	82	468.7
TGS-5-1	100×80×75	6	8	30	40	235	92	467.3
TGS-5-2	100×90×75	6	8	30	40	235	92	468.5
TGS-5-4	100×110×75	6	8	30	40	235	92	463.5
TGS-6-2	100×100×75	6	8	40	40	235	92	482.8
TGS-6-3	100×100×75	6	8	50	40	235	92	486.5
TGS-6-4	100×100×75	6	8	60	40	235	92	489.2
TGS-6-5	100×100×75	6	8	70	40	235	92	489.6
TGS-7-1	100×100×75	6	8	30	30	235	92	452.1
TGS-7-3	100×100×75	6	8	30	50	235	92	486.2
TGS-7-4	100×100×75	6	8	30	60	235	92	500.6
TGS-7-5	100×100×75	6	8	30	70	235	92	507.6
TGS-8-2	100×100×75	6	8	30	40	275	92	495.9
TGS-8-3	100×100×75	6	8	30	40	355	92	527.4
TGS-8-4	100×100×75	6	8	30	40	390	92	540.0
TGS-8-5	100×100×75	6	8	30	40	420	92	553.9
TGS-8-6	100×100×75	6	8	30	40	460	92	566.2

Note: TGS-1-1 is regarded as a standard part, which is the same parameter as TGS-3-2, TGS-4-6, TGS-5-3, TGS-6-1, TGS-7-2 and TGS-8-1, so only one set of data is listed.

5. Calculation of shear bearing capacity

5.1. Calculating methods of shear bearing capacity

Nie et al. [28] analyzed the mechanical behaviors of 49 channel steel connectors and proposed an equation:

$$P_u = (0.6df_y + (6t + 0.15b)f_c)L \tag{1}$$

where d and t are the web and flange thickness, b is the flange width, L is the channel steel length, f_y and f_c are the steel yield strength and concrete compressive strength, P_u is the shear bearing capacity.

The Code for design of steel and concrete composite bridges [29] provided an equation to calculate the bearing capacity of a channel steel that considers the simultaneous shear forces on the channel web and flange as follows:

$$P_u = 0.26(t + 0.5t_w)L\sqrt{E_c f_c} \tag{2}$$

where t and t_w are the flange average thickness and web thickness, L is the channel steel length, f_c and E_c are the concrete compressive strength and elastic modulus.

The shear bearing capacity calculation equation given in AISC/ANSI 360-10 [30] takes into account the impact of the flange thickness of angle steel connector on its shear strength as follows:

$$P_u = 0.3(t_f + 0.5t_w)L\sqrt{E_c f_c} \tag{3}$$

where t_f, t_w and L are the average thickness flange, web thickness and angle steel length.

Notably, the equation given in Eurocode 4 [18] for obtaining the bearing capacity of angle steel does not consider the interaction between the connector and concrete, only considers the influence of the weld strength as follows:

$$P_u = \min(Q_{u1} = \frac{Af_c}{1.5}, Q_{u2} = aL\frac{f_y}{\sqrt{3}}) \tag{4}$$

where A is the angle steel area and a is the theoretical thickness of weld.

Comparing the T-shaped connector shear bearing capacity calculated using the national codes with the test and FEA results in Table 6, the results obtained using Eqs. (1)–(3) are clearly too conservative, Eqs. (2) and (3) do not consider the impact of the steel strength of connector on bearing capacity. Furthermore, the values obtained by Eq. (4) are higher than those determined by the FEA with considerable errors and dispersions. This occurred because the shape and size of T-shaped connector have different effects than those of the angle steel connector on shear capacity.

5.2. Calculation formula of shear bearing capacity

The equation for the shear bearing capacity of channel steel proposed by Nie [28] was modified by using the multiple linear regression analysis based on the FEA results given in Section 4 to obtain the following shear bearing capacity equation for the T-shaped connector:

$$P_u = (0.75t_w f_y + (0.52t + 0.96L)f_c)h \tag{5}$$

Table 6 compares the values calculated using Eq. (5) with those obtained by the experiment and FEA, indication suitable agreement with an average error less than 10% and a standard deviation of 0.23. Therefore, the calculation formula established in this paper can be used for predicting the shear capacity of the T-shaped shear connector.

Table 6
Comparison results of shear bearing capacity

Number	$P_{u,t}$(kN)	Mean value	μ_1	μ_2	μ_3	μ_4	μ
TGS-1-1	236.4		0.65	0.71	0.82	1.76	0.97
TGS-1-2	245.7		0.67	0.72	0.83	1.70	1.00
TGS-1-3	275.5		0.63	0.67	0.77	1.53	0.95
TGS-1-4	292.8		0.63	0.66	0.76	1.45	0.95
TGS-1-5	311.1		0.63	0.64	0.74	1.37	0.95
TGS-1-6	329.8		0.63	0.63	0.73	1.30	0.94
TGS-1-7	346.6		0.63	0.62	0.72	1.24	0.94
TGS-1-8	362.8		0.63	0.61	0.71	1.19	0.95
TGS-1-9	360.3		0.66	0.64	0.74	1.21	1.00
TGS-2-1	236.6		0.71	0.58	0.67	1.74	1.18
TGS-2-2	243.6		0.73	0.63	0.73	1.70	1.15
TGS-2-3	263.7		0.71	0.64	0.74	1.58	1.06
TGS-2-4	271.1		0.72	0.68	0.78	1.55	1.04
TGS-2-5	277.3		0.73	0.72	0.83	1.52	1.02
TGS-2-6	279.7		0.76	0.77	0.89	1.51	1.01
TGS-2-7	279.1		0.79	0.83	0.95	1.53	1.02
TGS-2-8	278.8		0.82	0.88	1.02	1.54	1.02
TGS-2-9	278.3		0.85	0.94	1.08	1.55	1.03
TGS-3-1	222.2		0.60	0.66	0.76	1.64	0.96
TGS-3-3	246.9		0.71	0.78	0.90	1.89	1.00
TGS-3-4	269.6		0.72	0.79	0.92	1.92	0.98
TGS-4-1	204.4		0.75	0.83	0.95	2.04	0.51
TGS-4-2	224.7		0.68	0.75	0.87	1.85	0.58
TGS-4-3	233.2		0.66	0.72	0.84	1.79	0.67
TGS-4-4	233.2		0.66	0.72	0.84	1.79	0.77

TGS-4-5	234.4		0.66	0.72	0.83	1.78	0.88
TGS-5-1	233.7		0.64	0.72	0.83	1.78	0.99
TGS-5-2	234.3		0.65	0.72	0.83	1.78	0.98
TGS-5-4	231.8		0.67	0.73	0.84	1.80	0.99
TGS-6-2	241.4		0.64	0.70	0.81	1.73	0.95
TGS-6-3	243.3		0.63	0.69	0.80	1.71	0.95
TGS-6-4	244.6		0.63	0.69	0.80	1.70	0.94
TGS-6-5	244.8		0.63	0.69	0.80	1.70	0.94
TGS-7-1	226.1		0.58	0.62	0.72	1.38	0.87
TGS-7-3	243.1		0.71	0.79	0.91	2.07	1.06
TGS-7-4	250.3		0.77	0.85	0.98	2.40	1.16
TGS-7-5	253.8		0.84	0.92	1.06	2.73	1.26
TGS-8-2	248.0		0.66	0.68	0.79	1.68	1.00
TGS-8-3	263.7		0.71	0.64	0.74	1.58	1.06
TGS-8-4	270.0		0.72	0.63	0.72	1.54	1.09
TGS-8-5	277.0		0.74	0.61	0.70	1.50	1.11
TGS-8-6	283.1		0.76	0.60	0.69	1.47	1.14
AVE			0.69	0.71	0.82	1.68	0.97
STE			0.07	0.09	0.10	0.29	0.14
TG-1	255.7	273.05	0.77	0.66	0.76	1.93	1.39
TG-2	290.4						
TG-3	424.1	399.9	0.63	0.49	0.57	1.33	1.11
TG-4	375.8						
TG-5	384.2	362.7	0.64	0.59	0.68	1.47	0.83
TG-6	341.3						
TG-7	398.9	421.6	0.67	0.54	0.63	1.27	1.03
TG-8	444.3						
AVE			0.67	0.57	0.66	1.50	1.09
STE			0.06	0.06	0.07	0.26	0.23

Note: μ_1 to μ are the ratio of the calculated value obtained by Eq. (1) to Eq. (5) to $P_{u,t}$, respectively; AVE is the average value, STE is the standard deviation.

6. Conclusion

This study completed eight push-out tests and established larges of accurate numerical models on the T-shaped shear connectors in prefabricated concrete composite floor slabs to determine the effect of different parameters on their shear behavior, and put for word a design equation of shear bearing capacity. The following conclusions were obtained:

1) The T-shaped shear connector had a large initial stiffness and excellent ductility during the service stage. The characteristic slip values of the evaluated specimens were between 15.67 and 30.56 mm, meeting the requirements of Eurocode 4 for flexible connectors (> 6 mm).

2) The failure mode of each specimen exhibited shear failure at the connection between T-shaped shear connector and H-beam, obvious fracture between the H-beam and composite slab, and multiple cracks in the prefabricated concrete slab with a maximum width of 1.5 mm.

3) The section dimension of T-shaped connector and material strength had different degrees of impact on its shear capacity: the web thickness had the greatest influence whereas the connector width and prefabricated concrete compressive strength had almost no influence. On the premise of considering shear behavior, economy and structural requirements, some suggestions on the optimal selection of cross-section size of T-shaped connectors are given.

4) The results of extensive FEA simulations were analyzed using the multiple linear regression method to propose a formula for the shear bearing capacity of a T-shaped connector, which are expected to provide theoretical basis for the application of this shear connectors in prefabricated concrete composite floor system so as to improve the overall performance and economy of structures.

Acknowledgments

The investigation was supported by the National Key Research and Development Program of China (Grant No. 2017YFC0703407) and Shenyang Science and Technology Program of China (Grant No. 23503609).

References

[1] Yu S, Liu Y and Wang D. “Review of thermal and environmental performance of prefabricated buildings: Implications to emission reductions in China”. Renewable and Sustainable Energy Reviews, 137:110472, 2021.

[2] Li X, Xie W and Yang T. “Carbon emission evaluation of prefabricated concrete composite plates during the building materialization stage”. Building and Environment, 232, 110045, 2023.

[3] LI G, CAO K and YANG Z. “Finite Element Analysis of Steel Reinforced Concrete Stub Columns with New Shear Connectors under Axial Compression”. Journal of Shenyang Jianzhu University (Natural Science), 38(2):202-210, 2022. (in Chinese)

[4] Yossef M, Chen A and Elsayad M. “Deconstructable variable stiffness shear connectors in FRP deck resting on multigirder bridge system: Analytical model”. Engineering Structures, 307:117932, 2024.

[5] Jakovljević I, Spremić M and Marković Z. “Shear behaviour of demountable connections with bolts and headed studs”. Advanced Steel Construction (Accepted for Publication on 16th May 2023), 2023.

[6] Xu Q, Sebastian W and Lu K. “Development and Performance of Innovative Steel Wedge Block–Crossed Inclined Stud–UHPC Connections for Composite Bridge”. Journal of Structural Engineering, 148(9):04022128, 2022.

[7] Shariati A T A. “Monotonic behavior of C and L shaped angle shear connectors within steel-concrete composite beams: an experimental investigation”. Steel & Composite Structures: An International Journal, 35(2):237-247, 2020.

[8] Viest I M. “Full-scale tests of channel shear connectors and composite t-beams”. University of Illinois at Urbana-Champaign, 1951.

[9] Shariati M, Sulong N H R and Suhatril M. “Comparison of behaviour between channel and angle shear connectors under monotonic and fully reversed cyclic loading”. Construction and Building Materials, 38(38):582-593, 2013.

[10] Haroon M, Lee H D and Shin K J. Performance of angle shear connectors for U-shaped steel concrete infilled composite beams. Heliyon, 10(3): e25119, 2024.

[11] Arévalo D, Hernández L and Gómez C. “Structural performance of steel angle shear connectors with different orientation”. Case Studies in Construction Materials, 14: e00523, 2021.

[12] Hajime O, Yoshio K. “JSCE Research Subcommittee on Steel-Concrete Sandwich Structures”. Design code for steel-concrete sandwich structures–Draft, 20:1-21, 1992.

[13] ZHOU W, BAI J and LEI Y. “Experimental study on the lattice type of angle steel connectors──the fourth of the series of studies on steel-concrete composite truss”. Journal

of Hefei University of Technology (Natural Science Edition), (02):126-130, 1994. (in Chinese)

[14] CUI J, ZHANG X. "The Study of Composite Beam Flexural Test and Shear Strength of Angle Connectors. Journal of Anhui Jianzhu University, 31(01):1-9, 2023. (in Chinese)

[15] TANG L, FAN J and NIE J. "Experimental study on the mechanical performance of angle shear connectors with and without concrete gaps". Engineering Mechanics, 37(10): 45-55+115, 2020. (in Chinese)

[16] Soty R, Shima H. "Formulation for shear force–relative displacement relationship of L-shape shear connector in steel–concrete composite structures". Engineering Structures, 46:581-592, 2013.

[17] WANG X, DENG W and ZHANG J. "Mechanical characteristics of shear connectors under repeated loads". Journal of Jiangsu University of Technology (Natural Science Edition), 39(06):708-713, 2018. (in Chinese)

[18] EN1994-1-1, "Eurocode 4: Design of composite steel and concrete structures. Part 1-1: General rules and rules for buildings". Brussels: CEN; 2004.

[19] QIU Z. "Development and Performance Study of New Connection between Prefabricated Concrete Laminated Floor Slab and Steel Beam". Shenyang: Shenyang Jianzhu University, 2014. (in Chinese)

[20] YAN Y, DENG P and HOU H. "Experimental study on shear resistance of bolt connector in steel-concrete composite beam". Journal of Shandong University of Science and Technology (Natural Science), 40(02): 51-59, 2021. (in Chinese)

[21] YANG Y, ZHANG S and CHEN X. "Experimental study on the shear behavior of a bolt connector in a steel-concrete composite beam". Journal of Harbin Engineering University. 45(06):1076-1084, 2024. (in Chinese)

[22] GB 50010—2010, "Code for design of concrete structures". China Architecture & Building Press, Beijing, 2010. (in Chinese)

[23] LI G, WANG Z and YANG Z. "Experimental study on shear behavior of π-type crestbond shear connectors". Journal of Building Structures, 43(06):75-86, 2022. (in Chinese)

[24] Luo Y B, Sun S K and Yan J B. "Shear behavior of novel demountable bolted shear connector for prefabricated composite beam". Advanced Steel Construction, 18(4):745-752, 2022.

[25] REN C, YUAN Y, CHEN Y. "Finite Element Analysis on Shear Performance Large-Diameter Short Stud Connectors in Prefabricated Steel-Thin UHPC Composite Beams". Industrial Construction, 53(11):180-187, 2023. (in Chinese)

[26] Yan J B, Zhang W. "Numerical analysis on steel-concrete-steel sandwich plates by damage plasticity model: From materials to structures". Construction and Building Materials, 149: 801-815, 2017.

[27] GB/T 706-2016, "Hot rolled section steel. Standards Press of China", Beijing, 2016. (in Chinese)

[28] NIE J, SUN G. "Study on steel channel shear connector of steel-concrete composite beams". Industrial Construction, (10):8-13+57, 1990. (in Chinese)

[29] GB 50917-2013, "Code for design of steel and concrete composite bridges". China Planning Press, Beijing, 2013. (in Chinese)

[30] ANSI/AISC 360-10, "AISC. Specification for structural steel buildings", American Institute of Steel Construction, Chicago, Illinois, 2010.